

# Low-lying eigenmodes of the Wilson-Dirac operator and correlations with topological objects

Daniel-Jens Kusterer<sup>1</sup>, John Hedditch<sup>2</sup>, Waseem Kamleh<sup>3</sup>,  
Derek B. Leinweber<sup>4</sup> and Anthony G. Williams<sup>5</sup>

*CSSM Lattice Collaboration, Special Research Center for the Subatomic Structure of Matter (CSSM) and Department of Physics and Mathematical Physics, University of Adelaide 5005, Australia*

---

## Abstract

The probability density of low-lying eigenvectors of the hermitian Wilson-Dirac operator  $H(\kappa) = \gamma_5 D_W(\kappa)$  is examined. Comparisons in position and size between eigenvectors, topological charge and action density are made. We do this for standard Monte-Carlo generated SU(3) background fields and for single instanton background fields. Both hot and cooled SU(3) background fields are considered. An instanton model is fitted to eigenmodes and topological charge density and the sizes and positions of these are compared.

*Key words:* Lattice, Eigenmodes, Wilson-Dirac operator, Topology, Instantons

---

## 1 Introduction

It is known [1,2,3,4,5] that the zero modes of lattice Dirac operators are strongly localised. We show that not only zero modes but all low-lying modes of the hermitian Wilson-Dirac operator  $H(m_0) = \gamma_5 D_W(-m_0)$  are strongly localised for bare quark masses  $0 \leq m_0 \leq 2$ . Furthermore, we show that this localization is strongly correlated to topological objects, including instantons.

<sup>1</sup> E-Mail: djkuster@physics.adelaide.edu.au

<sup>2</sup> E-Mail: jhedditc@physics.adelaide.edu.au

<sup>3</sup> E-Mail: wkamleh@physics.adelaide.edu.au

<sup>4</sup> E-Mail: dleinweb@physics.adelaide.edu.au

<sup>5</sup> E-Mail: awilliam@physics.adelaide.edu.au

A similar examination has been done for the overlap formalism [6]. We are interested in examining the extent to which similar properties are already manifested at the kernel level of the overlap formalism.

Our Wilson-Dirac operator is defined in the standard way by

$$\begin{aligned}
 [D_W(\kappa)\psi](x) = & \psi(x) - \kappa \sum_{\mu} [(1 - \gamma_{\mu})U_{\mu}(x)\psi(x + \mu) \\
 & + (1 + \gamma_{\mu})U_{\mu}^{\dagger}(x - \mu)\psi(x - \mu)],
 \end{aligned}
 \tag{1}$$

where the hopping parameter  $\kappa$  is related to the bare mass by

$$\kappa = (8 - 2m_0)^{-1}.
 \tag{2}$$

Therefore the above mentioned bare mass range is equivalent to  $0.125 \leq \kappa \leq 0.25$  at tree level. We examine eigenmodes in and just outside the region  $m_c < m_0 < 2$ , where  $m_c$  is the ‘‘critical-mass’’ which is 0 at tree-level but for non-trivial gauge fields shifts away from 0. This is the range of the mass parameter  $m_0$  needed for use in the overlap formalism. Modes of  $H(m_0)$  crossing zero in this region are accompanied by the abrupt appearance of exact zero modes of the overlap-Dirac operator at the corresponding  $m_0$  value [7].

We solve the eigenvalue problem  $D_W\psi(x) = \lambda\psi(x)$  for the first four low-lying eigenvalues. We are interested in calculating eigenmodes in the physical region of the overlap formalism with some further points just at the edge of this region. This corresponds to a  $\kappa$ -region starting slightly below the critical value of  $\kappa = \kappa_c$  and extending slightly beyond the point where doublers appear in the continuum limit of the overlap formalism. We consider  $0.115 \leq \kappa \leq 0.26$  at tree level. Since the critical  $\kappa$ -value shifts from its free field value of 0.125 to some higher value for non-zero gauge coupling, we have to adjust our  $\kappa$ -range accordingly. We look for any change in behaviour of the eigenmodes at the border of the region of physical interest.

Eigenmodes are found by an accelerated conjugate gradient routine [8] which is further improved by using dynamic state renormalisation. The major advantage of a conjugate gradient algorithm besides its almost perfect parallel structure is that it yields not only eigenvalues with appropriate degeneracies, but eigenvectors, as well. For selected  $\kappa$ -values we also calculate up to 20 eigenmodes. In the following, the phrase ‘‘low-lying eigenmodes’’ should be understood to mean eigenmodes corresponding to the low-lying eigenvalues.

In order to examine localisations of calculated eigenmodes we plot the probability density  $\rho(x) = \|\psi(x)\|^2$  for three dimensional cuts through the lattice. For comparison we plot the action density as well as the topological charge density for the appropriate configuration in the same way. Our calculations are

made on  $8^3 \times 16$ ,  $16^4$  and  $16^3 \times 32$  lattices with anti-periodic fermion boundary conditions in the time direction. On the  $8^3 \times 16$  lattice we test the correlation of low-lying eigenmodes with a single instanton configuration and standard Monte-Carlo generated SU(3) background fields. For the latter background fields we consider hot, 5-sweep and 12-sweep cooled configurations. Calculations on the larger lattices are to verify the conclusions we obtain from the smaller lattice. In order to quantify our results further we fit an instanton model to the obtained data. We distinguish between the model for action or charge densities and the model for the zero-mode density [9],

$$p(x)_{\text{act}} = c \cdot \frac{6}{\pi^2} \cdot \frac{\rho^4}{((x - x_0)^2 + \rho^2)^4}, \quad (3)$$

$$p(x)_{\text{zero}} = c \cdot \frac{2}{\pi^2} \cdot \frac{\rho^2}{((x - x_0)^2 + \rho^2)^3}, \quad (4)$$

where  $x$  is the distance from the instanton peak at  $x_0$  to the calculated densities. The normalisation factor  $c$  allows us to fit to the instanton shape and prevents the fit from being dominated by the maximal value of the fitted object which is affected by periodic images due to the finite volume of the 4-torus. Both models are continuum results derived from the standard 't Hooft ansatz. Eq. (3) is the action density and is used to fit action and charge densities. Eq. (4) is the density of the fermion field in the zero-mode and is used to fit eigenmode densities. This allows us to compare localisation sizes and positions quantitatively.

This paper is organised as follows: After a discussion in Sec. 2 of lattice techniques and general properties, we describe results for a single instanton configuration on a  $16^4$  lattice in Sec. 3. In Sec. 4 we investigate localisations of eigenmodes of the hermitian Wilson-Dirac operator and the correlations those eigenmodes have with topology on standard Monte-Carlo generated SU(3) configurations on a  $16^3 \times 32$  lattice. We do this for both hot and 12-sweep-cooled configurations. We quantify those localisations and their correlations to topology and compare sizes of the eigenmode localization with sizes of the corresponding topological object in Sec. 5. Conclusions are presented in Sec. 6.

## 2 Lattice techniques

We carry out our studies on three different lattices. Single instanton configurations are created on an  $8^3 \times 16$  lattice with  $\rho = 1.0$  and on a  $16^4$  lattice with  $\rho = 2.0$ . The latter configuration is cooled for 2 sweeps using the standard Wilson action to minimize boundary effects. We consider three standard Monte-Carlo SU(3) configurations generated on an  $8^3 \times 16$  lattice with

$\beta = 4.38$ , which corresponds to a lattice spacing of 0.165(2) fm. The second lattice size used is  $16^3 \times 32$  with  $\beta = 4.60$  which corresponds to a lattice spacing of 0.125(2) fm. These configurations are generated with a plaquette plus rectangle improved action with mean-field improved coefficients. For the smaller exploratory lattice the standard Wilson action and standard plaquette topological charge are used to minimize boundary effects. For the bigger lattice, a three-loop improved action and three-loop improved topological charge operator [10,11] are used.

The topological charge density is given by

$$q(x) = \frac{g^2}{32\pi^2} \epsilon_{\mu\nu\rho\sigma} \text{Tr}(F_{\mu\nu}(x)F_{\rho\sigma}(x)). \quad (5)$$

For the standard plaquette topological charge we use the traceless definition of  $F_{\mu\nu}$  extracted from the consideration of  $1 \times 1$  plaquettes alone [12]

$$F_{\mu\nu} = \frac{-i}{8} \left[ W^{1 \times 1} - W^{1 \times 1 \dagger} \right]_{\text{Traceless}} \quad (6)$$

where  $W^{1 \times 1}$  is the clover-sum of four  $1 \times 1$  Wilson loops lying in the  $\mu, \nu$  plane. For the three-loop improved topological charge operator, we employ an  $\mathcal{O}(a^4)$  improved definition of  $F_{\mu\nu}$  in which the standard clover-sum of four  $1 \times 1$  Wilson loops lying in the  $\mu, \nu$  plane is combined with  $2 \times 2$  and  $3 \times 3$  Wilson loop clovers. Bilson-Thompson *et al.* [10] find

$$F_{\mu\nu} = \frac{-i}{8} \left[ \left( \frac{3}{2} W^{1 \times 1} - \frac{3}{20u_0^4} W^{2 \times 2} + \frac{1}{90u_0^8} W^{3 \times 3} \right) - \text{h.c.} \right]_{\text{Traceless}} \quad (7)$$

where  $W^{n \times n}$  is the clover-sum of four  $n \times n$  Wilson loops and where  $F_{\mu\nu}$  is made traceless by subtracting 1/3 of the trace from each diagonal element of the  $3 \times 3$  colour matrix. This definition reproduces the continuum limit with  $\mathcal{O}(a^6)$  errors. On approximately self-dual configurations, this operator produces integer topological charge to better than 4 parts in  $10^4$ .

We use periodic boundary conditions in space and anti-periodic in the time direction for fermions. Each of the hot configurations is also cooled for 12 sweeps using a Cabibbo Marinari based algorithm in which the three diagonal SU(2) subgroups of SU(3) are looped over twice [12] using a three-loop  $\mathcal{O}(a^4)$  improved action [10,11]. Twelve sweeps of cooling is just enough to see clear structure on the topological charge and action densities, but it still preserves much of the original topology. To see correlations for some eigenmode densities we also need to use the topological charge density of 5-sweep cooled configurations. These topological charge densities are much rougher, but are

closer to the original configuration, with topological objects moving less than in the 12-sweep cooled configurations.

The visualisations of the eigenmode probability densities are treated consistently in order to allow direct comparison. This means they are all normalised with respect to the maximum value of each eigenmode. In this way, an isosurface at half the peak height will reflect the size of the object.

### 3 Smooth instanton background

We generate a single instanton background on an  $8^3 \times 16$  and on a  $16^4$  lattice by performing the path integration of

$$A_\mu(x) = \frac{x^2}{x^2 + \rho^2} \left( \frac{i}{g} \right) (\partial_\mu S) S^{-1}, \quad (8)$$

with

$$S = \frac{x_4 \pm i \vec{x} \cdot \vec{\sigma}}{\sqrt{x^2}}, \quad (9)$$

where  $+$  is an instanton and  $-$  an anti-instanton, to create the link variable. We find in the regular gauge

$$U_\mu^{\text{reg}}(x) = \exp \left[ i a_\mu(x) \cdot \sigma \phi_\mu(x; \rho) \right], \quad (10)$$

$$\phi_\mu(x; \rho) = \frac{1}{\sqrt{\rho^2 + \sum_{\nu \neq \mu} (x_\nu - \bar{x}_\nu)^2}} \tan^{-1} \frac{\sqrt{\rho^2 + \sum_{\nu \neq \mu} (x_\nu - \bar{x}_\nu)^2}}{\rho^2 + \sum_{\nu} (x_\nu - \bar{x}_\nu)^2 + (x_\nu - \bar{x}_\nu)}, \quad (11)$$

$$\begin{aligned} a_1(x) &= (-x_4 + \bar{x}_4, x_3 - \bar{x}_3, -x_2 + \bar{x}_2), \\ a_2(x) &= (-x_3 + \bar{x}_3, -x_4 + \bar{x}_4, x_1 - \bar{x}_1), \\ a_3(x) &= (x_2 - \bar{x}_2, -x_1 + \bar{x}_1, -x_4 + \bar{x}_4), \\ a_4(x) &= (x_1 - \bar{x}_1, x_2 - \bar{x}_2, x_3 - \bar{x}_3). \end{aligned} \quad (12)$$

In the singular gauge we find<sup>6</sup>

$$U_\mu^{\text{sing}}(x) = \exp \left[ i b_\mu(x) \cdot \sigma (\phi_\mu(x; 0) - \phi_\mu(x; \rho)) \right], \quad (13)$$

<sup>6</sup> Note that the analogous result of [3] inverts the roles of instantons and anti-instantons

$$\begin{aligned}
b_1(x) &= (x_4 - \bar{x}_4, x_3 - \bar{x}_3, -x_2 + \bar{x}_2), \\
b_2(x) &= (-x_3 + \bar{x}_3, x_4 - \bar{x}_4, x_1 - \bar{x}_1), \\
b_3(x) &= (x_2 - \bar{x}_2, -x_1 + \bar{x}_1, x_4 - \bar{x}_4), \\
b_4(x) &= (-x_1 + \bar{x}_1, -x_2 + \bar{x}_2, -x_3 + \bar{x}_3).
\end{aligned}
\tag{14}$$

The singular gauge instanton is clearly recognisable on the volume rendered action density plot as seen in Fig. 1 (a). The outer surface shown is half the peak height.

The results seen on the smaller exploratory lattice are also found on the  $16^4$  lattice. The instanton on the latter lattice is cooled for two sweeps to minimise boundary effects. Eigenmodes of this configuration are calculated for  $0.12 \leq \kappa \leq 0.27$  with an increment of 0.01 between values. The first four eigenvalues of the spectrum are shown in Fig. 2. We then evaluate the localisation of  $\rho(x)$  for the first three low-lying eigenmodes for each  $\kappa$ . This is done by plotting  $\rho(x)$  as seen in Fig. 1 for selected eigenmodes.

For eigenmodes with  $\kappa \ll \kappa_c = 0.125$  we find a rather uniform distribution of  $\rho(x)$  whereas eigenmodes for all  $\kappa_c < \kappa < 0.27$  are strongly localised. For the lowest eigenmode this localisation strongly corresponds to the localisation of the instanton in the action density plot as seen by comparing Fig. 1 (a) and Fig. 1 (b), (c). We therefore say the eigenmode displays strong correlation with the instanton. The size and shape of this correlation varies from broad with some wall like structures for  $\kappa \leq \kappa_c$  to very small for  $\kappa_c < \kappa < 0.19$  and is getting broader again for larger values of  $\kappa$ . For higher eigenmodes this localization gets broader and less correlated with the instanton. Some higher eigenmodes show no correlation with the instanton but just wall like structure as seen in Fig. 1 (f). Others show prolate-like correlations as seen in Fig. 1 (d). Some eigenmodes also show a wall-like structure and a prolate-like correlation as seen in Fig. 1 (e). It is useful to note that plane wave behaviour would display uniform behaviour in the density plot.

#### 4 Monte-Carlo generated SU(3) gauge field background

After seeing that the low-lying eigenmodes of the Wilson-Dirac operator are strongly correlated to the instanton on a one-instanton configuration, we next carry out investigations on standard Monte-Carlo generated SU(3) background fields. We investigate three hot and three cooled configurations on both  $8^3 \times 16$  ( $\beta = 4.38$ ) and  $16^3 \times 32$  ( $\beta = 4.60$ ) lattices. Three-loop improved cooling [10,11] is used to cool the configurations for 12 sweeps. This is just enough to get clear structure in the action and topological charge. As a reference for comparison of the eigenmode density we use the action and topological charge

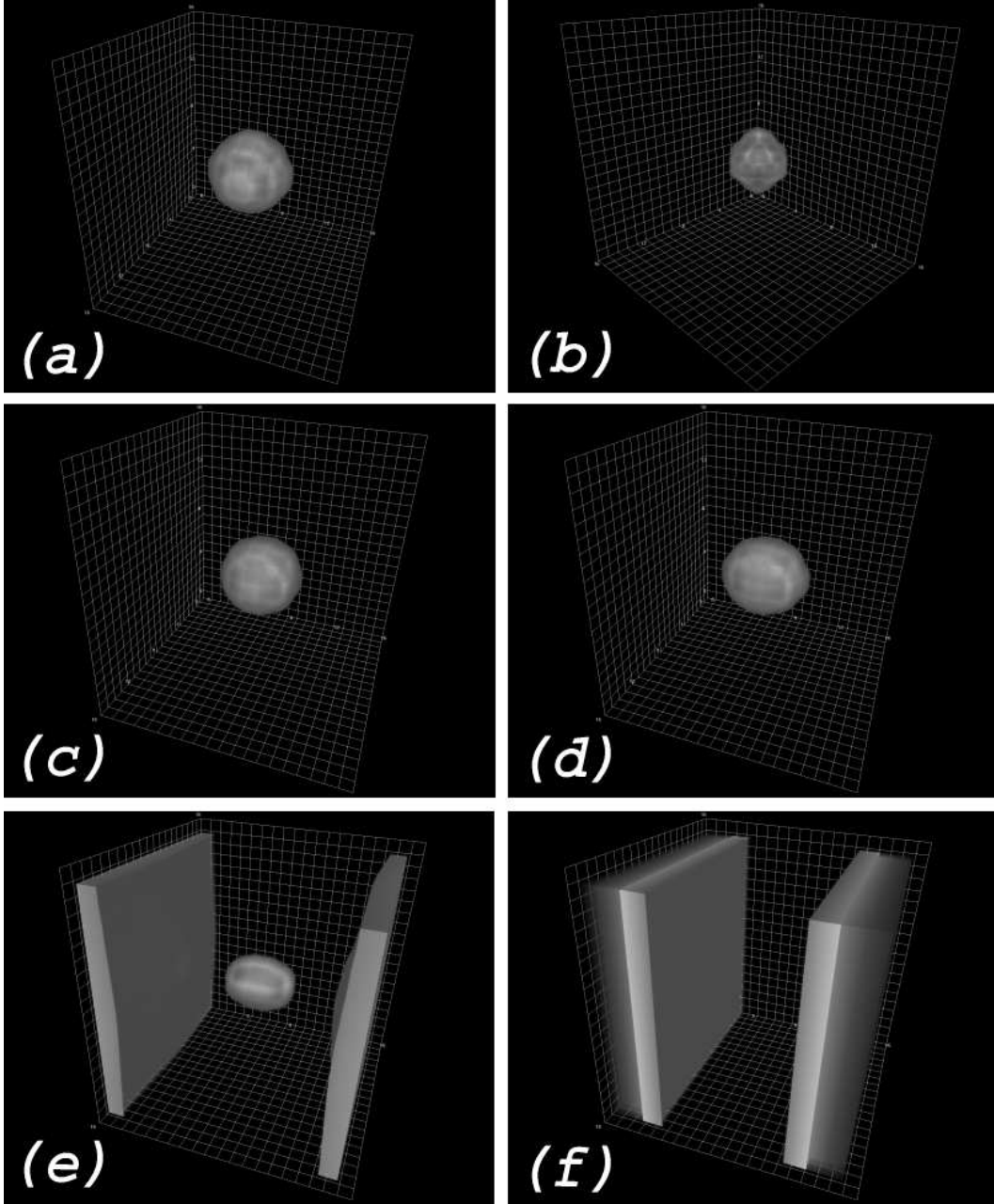


Fig. 1. (a) Action density of a single instanton configuration on a  $16^4$  lattice. (b) First eigenmode for the single instanton configuration for  $\kappa = 0.19$ . Note the very strong correlation with the instanton on the action density. (c) First eigenmode for the single instanton configuration for  $\kappa = 0.25$ . Again note the strong correlation between the eigenmode and the action density. (d) Second eigenmode for the single instanton configuration for  $\kappa = 0.25$ . The localization has a prolate shape compared to the spherical instanton. (e) Second eigenmode for the single instanton configuration for  $\kappa = 0.19$ . The localization has a wall like shape with a prolate correlation to the instanton. (f) Third eigenmode for the single instanton configuration for  $\kappa = 0.19$ . The eigenmode has a wall like shape and is not correlated with the instanton. For all figures what is shown is a volume rendering of the corresponding density. The outer isosurface is half the peak density.

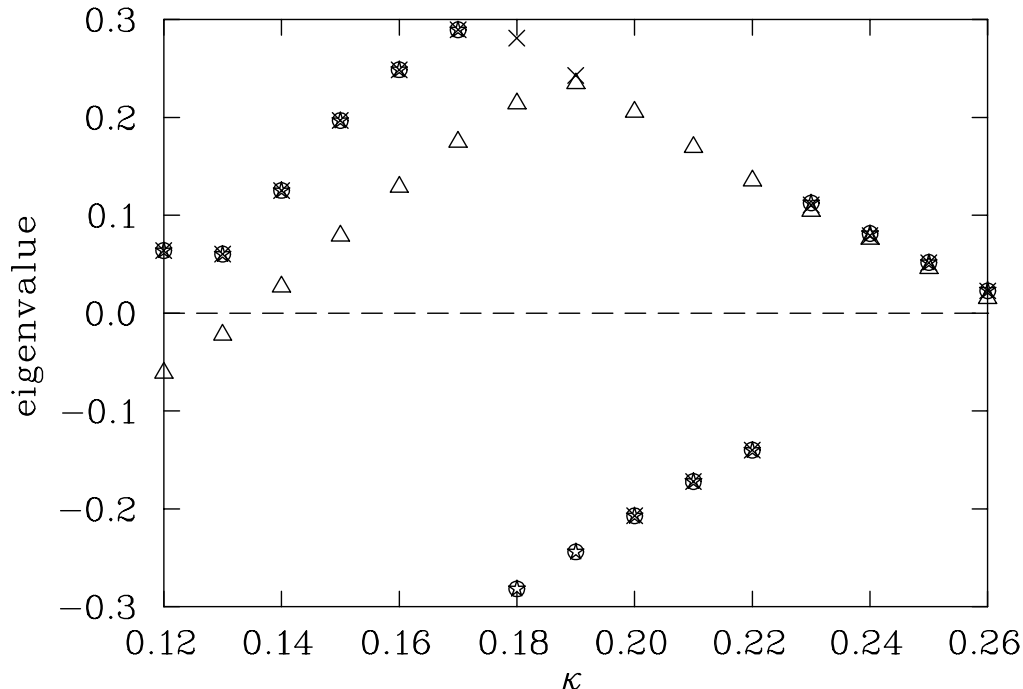


Fig. 2. Smallest four eigenvalues of the eigenvalue spectrum of a smooth single instanton configuration on a 2-sweep cooled  $16^4$  lattice. For the open triangles we have strong spherical correlation between the eigenmode and action density and behaviour as described in the text. For the other symbols we have correlation with prolate-like shapes and wall-like structures. The shapes are shown in Fig. 1. For  $\kappa = 0.20, 0.21$  and  $0.22$  we expect the fifth eigenvalue to lie degenerate with the open triangles.

density of the cooled configuration. We do this because those densities are too rough for the hot configuration and no accurate comparison would be possible. As there is more structure observed on the topological charge density plot, we use this as our preferred reference. See Fig. 4 (a) for a typical topological charge density plot of a  $16^3 \times 32$  configuration. However the action density plot is also useful for guidance.

We say an eigenmode is correlated to a topological object if  $\rho(x)$  has a peak within one lattice site of the peak topological charge density. We calculate the first four eigenmodes for values of  $0.13 \leq \kappa \leq 0.25$  for cooled configurations and  $0.15 \leq \kappa \leq 0.29$  for hot configurations in steps of 0.01. This range is from approximately 0.02 smaller than  $\kappa_c$  to a region where doublers appear in the overlap formalism. We find that the behaviour described in the following is general for all configurations: Each of the eigenmodes is localised. This was already observed for the lowest eigenmode [5]. For  $\kappa < \kappa_c$  this localization weakens and the density,  $\rho(x)$ , broadens quickly. An exponential decay of the density  $\rho(x)$ , as previously observed [2,5], seems likely to occur. All low-lying eigenmodes for  $\kappa \geq \kappa_c$  are correlated to topological objects.



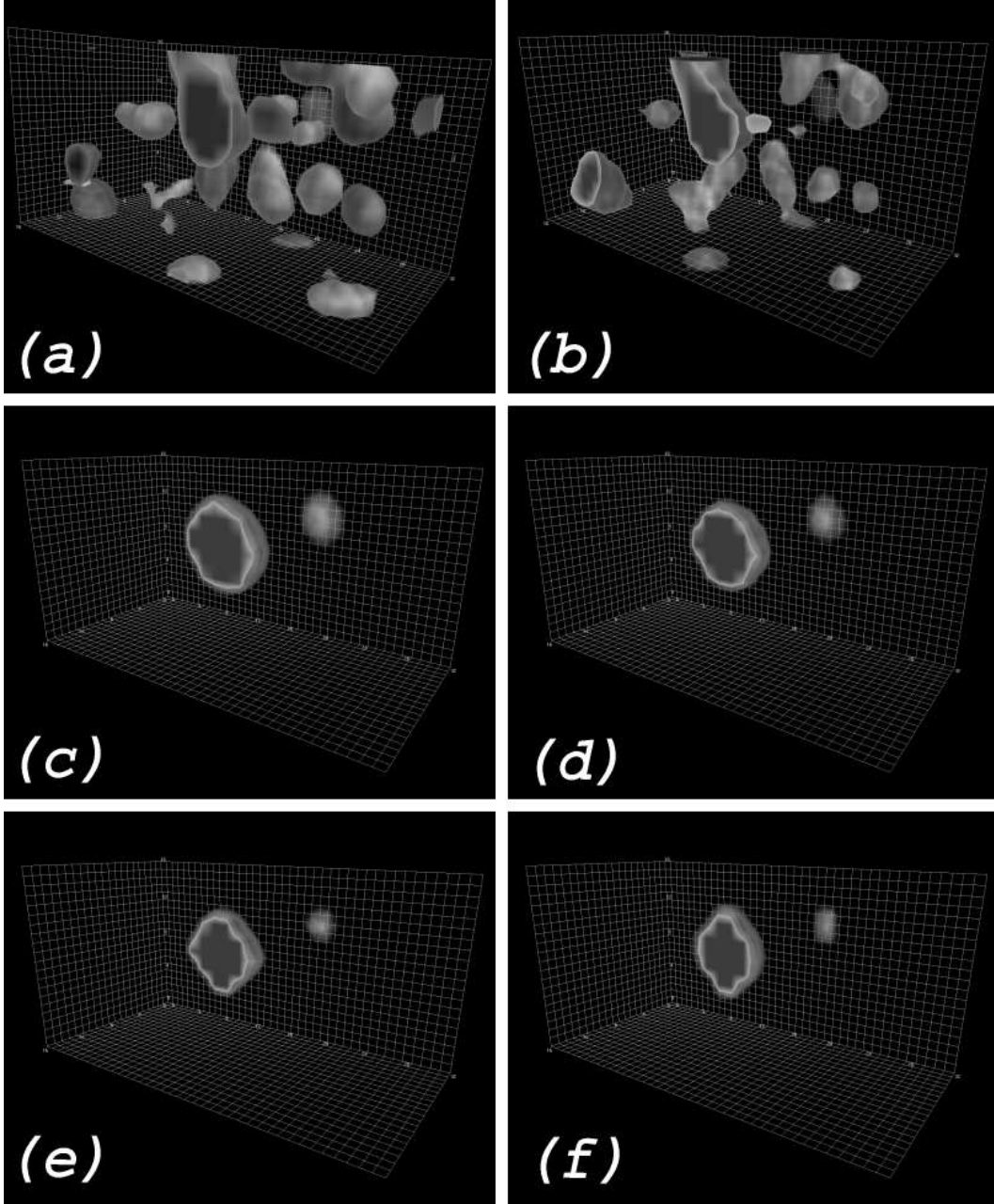


Fig. 4. (a) Topological charge density of a 12-sweep cooled  $16^3 \times 32$  configuration at  $\beta = 4.60$ . (b) Action density of the same configuration. There is clearly less structure for the action density than the topological charge density. (c) The low-lying eigenmode density at  $\kappa = 0.14$  of the same configuration with correlation to the object seen in the action density and the topological charge density. (d) Eigenmode density at  $\kappa = 0.16$  showing correlation to the same topological object. (e) Eigenmode density at  $\kappa = 0.18$ . The localization is maximal for this value of  $\kappa$ . (f) Eigenmode density at  $\kappa = 0.19$ . The localization is becoming larger again.

correlations to more than one topological object. In general we find that the closer the eigenvalues and the weaker the actual localisations, the more likely it is to get correlation with more than one topological object in the corresponding eigenmodes.

Calculations of 20 eigenmodes for selected values of  $\kappa$  on hot configurations show only little broadening in the localisations and persistent correlations with topology. This suggests that this behaviour will not change quickly and such correlations will persist for even higher eigenmodes.

As mentioned above, we use the topological charge density of the 12-sweep cooled configuration for comparison. The position of eigenmodes on cooled fields agree perfectly well with the position of topological objects seen in this density. A typical distance between such positions being 0.05 lattice units. For hot configurations some of the correlations are slightly offset compared to the structure in the smoothed configurations whereas other structure in the eigenmodes has no corresponding structure in the smoothed topological charge. But in those cases a comparison with a less cooled configuration reveals correlations between eigenmodes and topological objects which are moved or destroyed by further cooling. This behaviour is expected and understood, as topological objects are known to move under cooling as instantons and anti-instantons attract each other and annihilate when they are close enough together.

This clear correlation between  $\rho(x)$  of eigenmodes on hot configurations and topological objects suggests that it is possible to identify areas through the noise of a hot configuration with significant topology. We can “see through” the noise by using eigenmodes of the hermitian Wilson-Dirac operator.

The spectral plot of the first four eigenvalues of a 12-sweep cooled configuration looks different compared to the same plot on a hot configuration. Comparing Fig. 3 and Fig. 5 we notice the rhomboid shape with an area without any eigenvalues in the spectral plot of the cooled configuration. This is expected for such smoothed configurations [14]. Eigenmodes on the right-hand side of this rhomboid behave different than eigenmodes on the left-hand side of the rhomboid. The localization of the eigenmodes on the left-hand side is approximately the same as the localisations in the hot configuration. But the eigenmodes on the right-hand side are much weaker in localization. Those weaker localised eigenmodes are related to very high eigenmodes in the hot configuration and the process of cooling brings them into an area where we can observe them as low eigenmodes. These eigenmodes must be very high eigenmodes in a hot configuration for they are much weaker localised as localisations we have seen for up to the 20th eigenmode in a hot configuration. Although the behaviour in localization strength for eigenmodes of cooled configurations is different from that of eigenmodes of hot configurations the correlations with topological objects still exist for all eigenmodes. We will take a closer look at

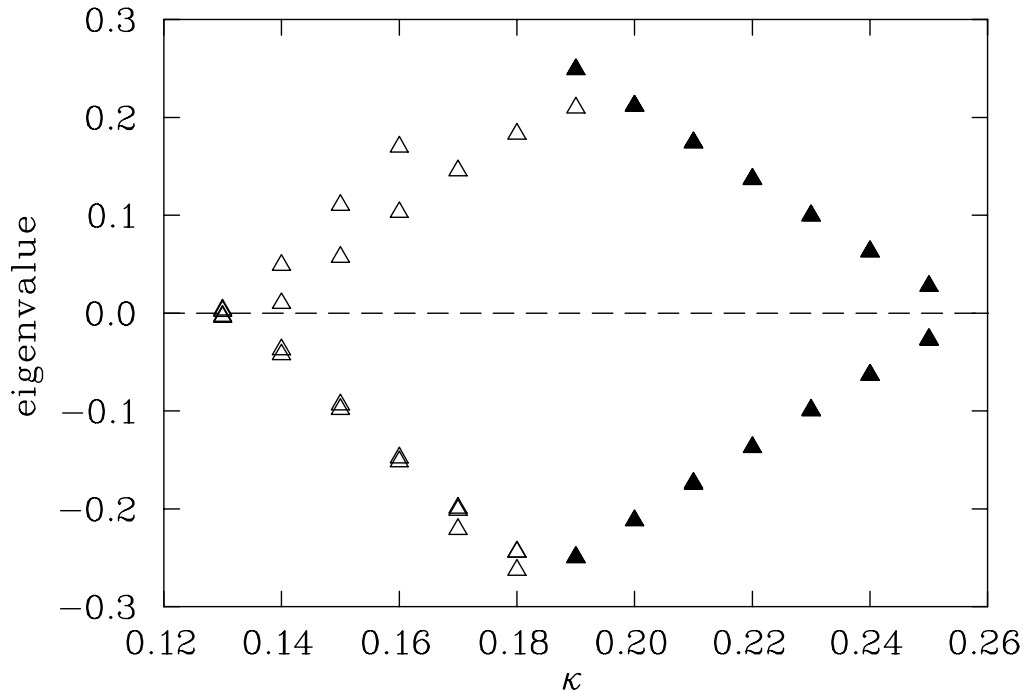


Fig. 5. First four eigenvalues of the spectrum of a 12-sweep cooled configuration. Note the rhomboid shape with the area without eigenvalues. The modes to the right of the maximum, the filled symbols, are only weakly localised. The open symbols are strongly localised.

localization strength and quantify it in the next section.

## 5 Quantitative Results

As described earlier in this paper, the localization of the eigenmodes change shape and size with changing of  $\kappa$ . In order to quantify this behaviour we have two methods. The first one is fairly simple. We have already seen that most eigenmodes are localized at one topological object. As the eigenmodes are all normalized, the maximum, or peak, value of the eigenmode density is an indicator of how strong this localization is. Fig. 6 shows the plot of such peak values for four eigenmodes each of three hot  $16^3 \times 32$  configurations. This plot shows a smooth behaviour with a maximum for  $\kappa_{\max} \approx 0.23$  for the lowest eigenmodes. This suggests that for hot SU(3) configurations the strongest localisation occurs in that  $\kappa$  region.

Fig. 7 shows the same plot for four eigenmode densities each for three 12-sweep cooled  $16^3 \times 32$  configurations. This plot shows a different behaviour. Again there is a clear peak, but the values drop to almost zero immediately after the peak. We expect this to happen after our qualitative observations in the previous section. These low maximum values correspond to weakly localized

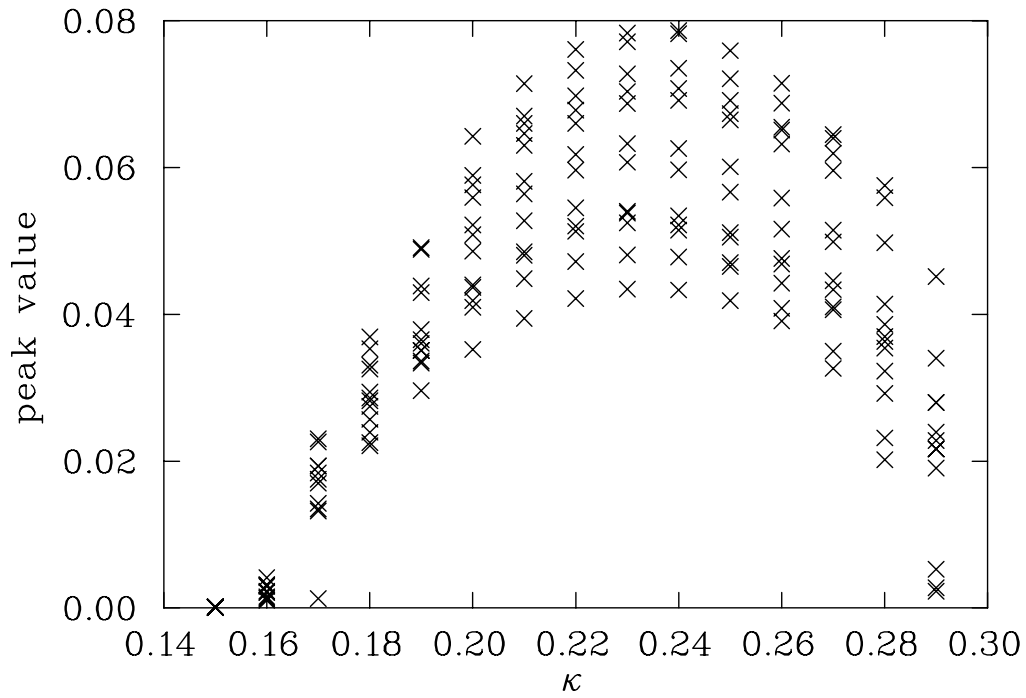


Fig. 6. Peak value of four eigenmode densities each from hot  $16^3 \times 32$  configurations with respect to  $\kappa$

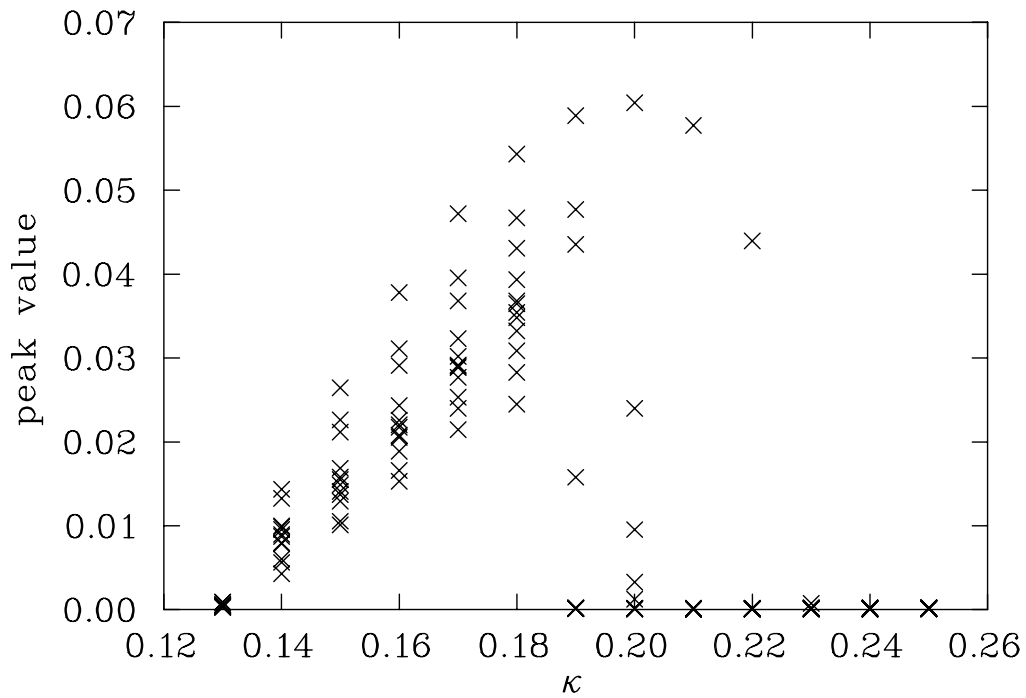


Fig. 7. Peak value of four eigenmode densities each from three 12-sweep cooled  $16^3 \times 32$  configurations with respect to  $\kappa$

modes, which are on the right-hand side of the spectrum shown in Fig. 5. In this case we can not determine  $\kappa_{\max}$ , for it is not clear how the localisations are going to develop if we follow the stronger localised eigenmodes up to higher values of  $\kappa$ . The one eigenmode we could follow suggests that  $\kappa_{\max} \approx 0.20$ . This reduction of  $\kappa_{\max}$  is about the same size as the reduction of  $\kappa_c$  for going from the hot to the 12-sweep cooled configuration.

To get more information about the shape of the eigenmodes, we fit the instanton model, Eq. (4), to the eigenmodes. This model gives us very good fits as

$$\sum_x (p(x)_{\text{zero}} - p_M(x))^2 = 10^{-5} \quad (15)$$

where  $p_M(x)$  is the 6 parameter fit of  $3^4$  points of  $p(x)$  centered about the peak of  $\rho(x)$ . This value is about 1000 times smaller than the peak value and  $10^{-5}$  is the worst case with most of the fits of order  $10^{-7}$  to  $10^{-9}$ . The fit parameter  $\rho$  is then a good measurement for the size of the localization.

In Fig. 8 we plot  $\rho(\kappa)$  for four eigenmodes calculated on all hot configurations and in Fig. 9 for four eigenmodes calculated on all 12-sweep cooled configurations. We see a behaviour which corresponds to the behaviour described above for the peak values of the eigenmodes.  $\rho(\kappa)$  for the hot configurations shows a smooth behaviour with a minimum around  $\kappa_{\max} = 0.26$ . This means the eigenmodes are maximally localised for this value of  $\kappa$  and are less localized for both ends of the spectrum. The  $\kappa_{\max}$  found this way varies slightly from  $\kappa_{\max}$  found by just taking the peak values of the eigenmode densities. It is about 0.03 larger at 0.26 for the lowest eigenmode. As we mentioned earlier the eigenmodes for low and high values of  $\kappa$  are localized on more than one topological object. Therefore Fig. 8 reports more local maxima than modes at these  $\kappa$ . However in the range  $0.18 \leq \kappa \leq 0.28$  only one local maximum is found per mode.

We have established that low-lying eigenmodes are correlated to a single topological object when eigenmodes are non degenerate. It is also established that an instanton gives rise to a zero crossing in the spectral flow with the sign of the slope equal to the sign of the topological charge [3]. However, as mentioned above, Fig. 3 reveals an eigenmode correlated to one topological object, but with two zero crossings. The size of the eigenmode varies from  $\rho = 1.2$  to  $\rho = 1.0$  as  $\kappa$  varies from 0.21 to 0.27. The size of the correlated object on the topological charge density, which can only be seen on the 5-sweep-cooled configuration, is  $\rho = 1.1$ . We have been able to reproduce similar spectral flows on single instanton configurations, which have been cooled with the Wilson action to the point where the topological charge is  $Q \approx 0.4$ , well below 1. Hence the double zero crossing of the spectral flow in Fig. 3 suggests the presence

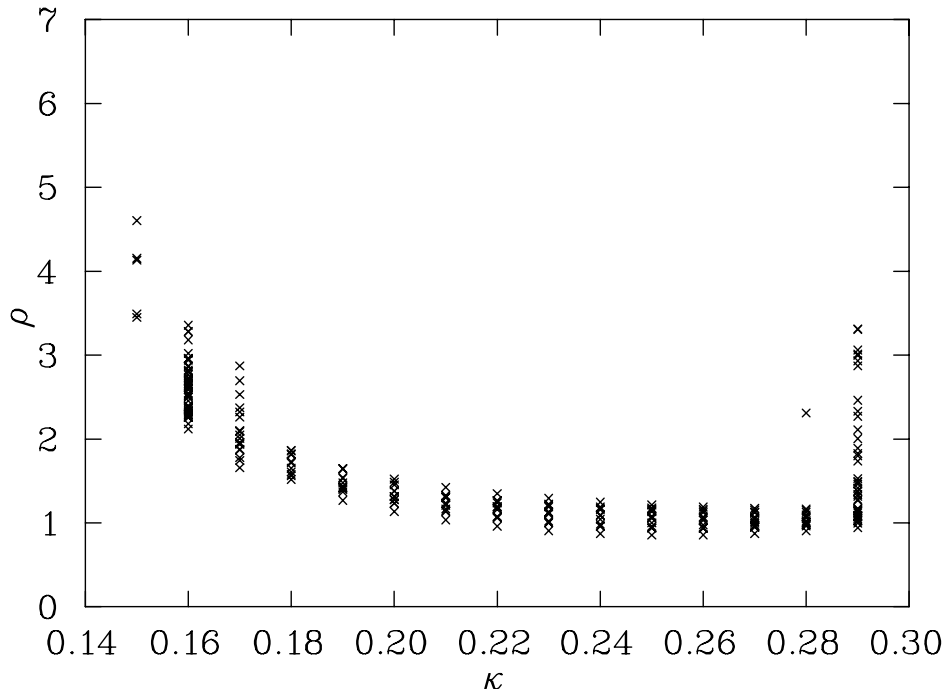


Fig. 8.  $\rho$  of the fitted instanton model of four eigenmodes from three hot  $16^3 \times 32$  configurations with respect to  $\kappa$ . Note that there are several correlations in one eigenmode at both ends of the spectrum.

of a lattice artifact. Ideally an improved fermion action should act to remove the zero crossings associated with this artifact.

The behaviour of  $\rho(\kappa)$  of the cooled configurations shows a jump at  $\kappa \approx 0.19$ , where the weakly localised modes set in as described above. Some of these weakly localised modes are not sufficiently localised to allow a fit to the instanton model. A fit would result in values for  $\rho \geq 10$ , which are not reasonable for the instanton model and therefore neglected. For those eigenmodes where we can do a fit, we get large values of  $\rho$  compared to the strongly localised eigenmodes. We find that  $\rho$  is about 2 for strongly localised eigenmodes and about 6 for weakly localised eigenmodes. For  $\kappa \leq 0.19$ ,  $\rho(\kappa)$  decreases smoothly, but for  $\kappa \geq 0.19$  the values of  $\rho(\kappa)$  are higher than at the lower end of the spectrum and do not show a smooth behaviour. Again it is hard to extract  $\kappa_{\max}$ , but it seems that if we could follow the stronger localised modes further it would be around 0.22. This is about 0.02 larger than the  $\kappa_{\max}$ , which is extracted using the peak values.

The fitting of the models to the eigenmode densities, using Eq. (4), as well as to the topological charge densities, using Eq. (3), allows us to compare the sizes for the eigenmode localisations with the sizes of the actual topological objects. In order to do this, we find the topological object which is located closest to the position of the eigenmode. We can fit the instanton model only to topological charge densities of cooled configurations, as only those are smooth

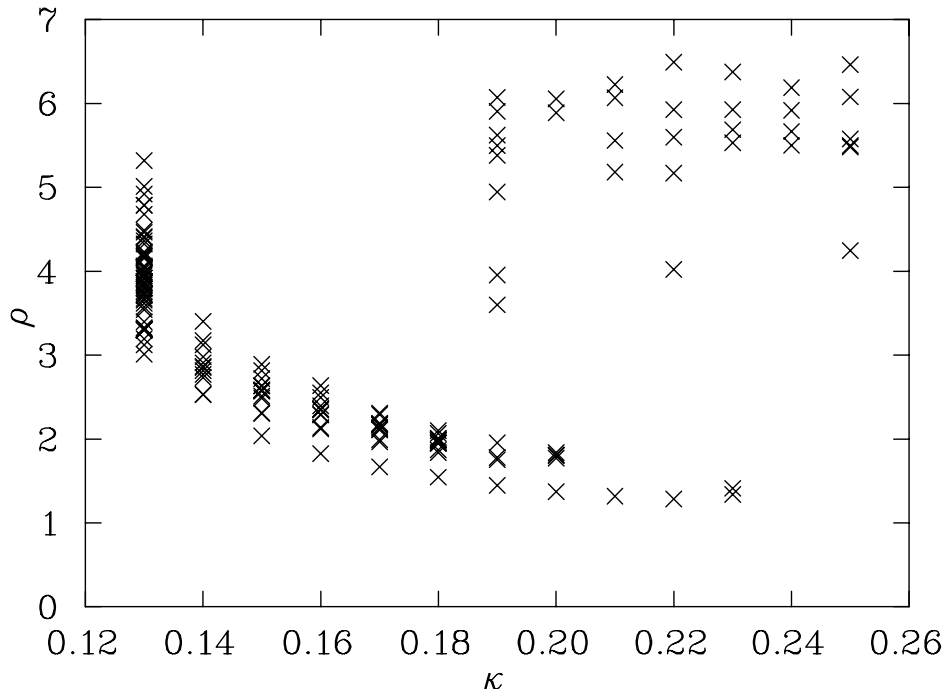


Fig. 9.  $\rho$  of the fitted instanton model of four eigenmodes from three 12-sweep cooled  $16^3 \times 32$  configurations with respect to  $\kappa$ . Note the jump at  $\kappa \approx 0.19$ .

enough. Therefore we only compare the sizes of eigenmodes of cooled configurations with sizes of actual topological objects. Due to the different localization strength for eigenmodes on the left-hand and on the right-hand side of the rhomboid spectrum of a cooled configuration, we look at those eigenmodes separately.

We find that the fitted positions for the strongly localised eigenmodes agree very well. With the fitted positions of the correlated topological objects lie within a fifth of a lattice spacing, and most of the times even better. The fitted positions of the weakly localised modes to the right of the spectrum agree only within one lattice spacing with their correlated topological objects. Strongly localised eigenmodes are correlated to smaller objects in the topological density. Such eigenmodes on the left-hand side of the eigenvalue spectrum, except those for  $\kappa \leq \kappa_c$ , have a size between  $\rho \approx 1.5$  and  $\rho \approx 3.5$ . The correlated topological objects have a size between  $\rho \approx 2$  and  $\rho \approx 3$ . The eigenmodes are larger than their correlated topological objects for smaller values of  $\kappa$ , but as they shrink with growing  $\kappa$  they get smaller than their correlated topological objects. All followed modes reach the size of the correlated topological object for  $0.155 < \kappa < 0.175$ . Fig. 10 shows an example of this behaviour.

The weakly localised eigenmodes on the right-hand side of the eigenvalue spectrum are larger than the strongly localised eigenmodes on the left-hand side of the spectrum. They turn out to have a size between  $\rho \approx 4$  and  $\rho \approx 6$ . But the topological charge density correlated with those eigenmodes are themselves

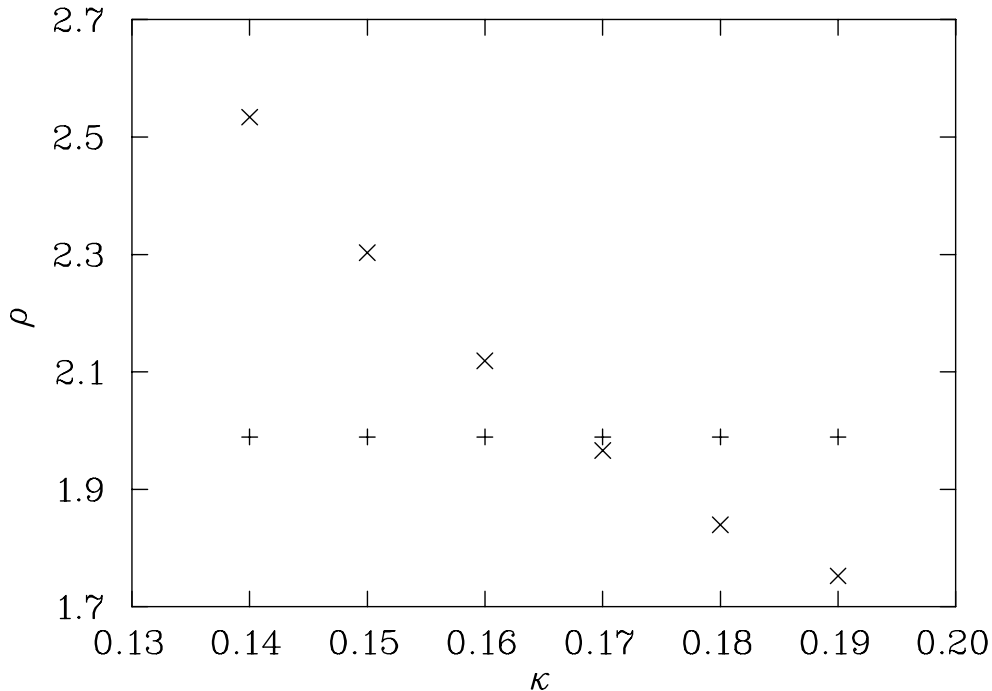


Fig. 10.  $\rho$  of the fitted instanton model of one mode of a 12-sweep cooled  $16^3 \times 32$  configuration with respect to  $\kappa$ . The  $\times$  denote the size of the eigenmode and the  $+$  denote the size of the correlated topological object. That the two graphs cross is a general result and all crossings are found for  $0.155 < \kappa < 0.175$ .

bigger than the topological charge density correlated with the stronger localised modes. The sizes of the topological charge density objects lie between  $\rho \approx 3$  and  $\rho \approx 4$ . The weaker localised eigenmodes are always bigger than the correlated topological objects with  $\rho_{\text{mode}} \approx \rho_{\text{topQ}} + 2$ .

For  $\kappa = \kappa_c$  the size of the eigenmodes is between  $\rho = 3$  and 5 with a relation to the size of the correlated topological objects of  $\rho_{\text{mode}} \approx \rho_{\text{topQ}} + 1$ . Sizes of strongly localised eigenmodes of hot configurations are of a comparable, but slightly smaller size than that on cooled configurations.

In order to understand why modes on the right-hand side of the rhomboid are just weakly localised we calculate spectra for one configuration with different amounts of cooling. We find that the value of  $\kappa$  where the jump in the localisation size occurs becomes smaller with cooling. Compare Fig. 9 and Fig. 11.

It is known [4] that zero crossings for larger  $\kappa$  correspond to smaller topological objects. As we see localisation sizes of calculated eigenmodes shrink with growing  $\kappa$  as well, we generally think of larger values of  $\kappa$  being associated with smaller objects. Cooling removes smaller objects first, therefore eigenmodes for large  $\kappa$  become “unassociated” with small objects. The eigenmodes show a behaviour of weak localisation which can be seen in Fig. 9 and Fig. 11

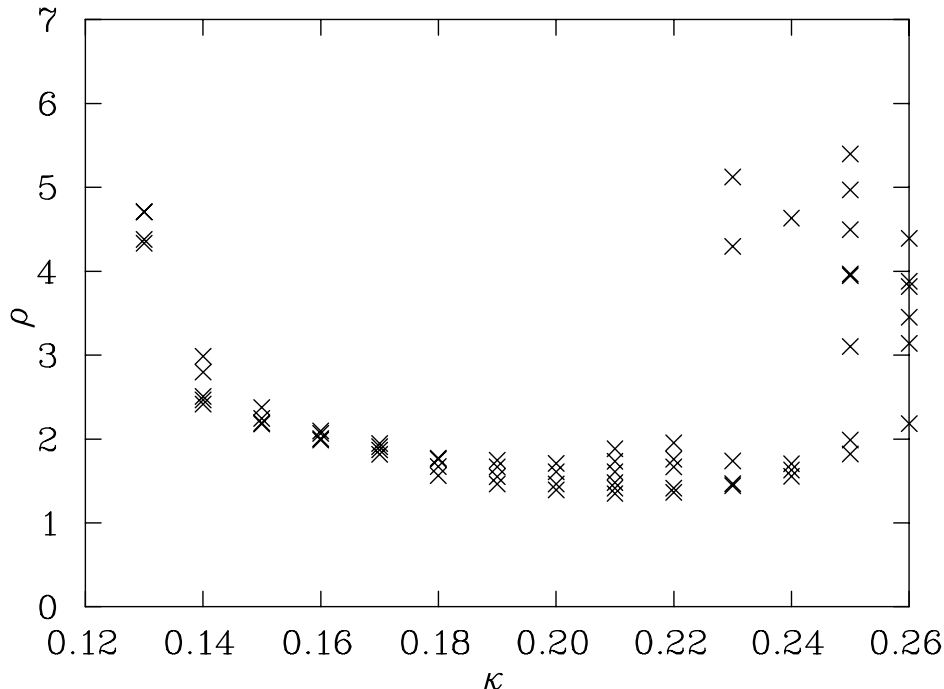


Fig. 11.  $\rho$  of the fitted instanton model of four eigenmodes for one 4-sweep cooled  $16^3 \times 32$  configuration with respect to  $\kappa$ . Note the jump occurring at higher  $\kappa$  compared to Fig. 9.

after the jump. Further cooling removes larger objects and therefore the value of  $\kappa$ , where the change of behaviour sets in, becomes smaller.

## 6 Conclusion

Not only zero modes, but all low-lying eigenmodes of the hermitian Wilson-Dirac operator  $D_W$  are strongly correlated to topological objects for  $\kappa \geq \kappa_c$ . These objects can be instantons for which  $S/S_0 = Q$  or topological fluctuations with  $S/S_0 > Q$ . One eigenmode is correlated to at least one topological object with correlations to more than one object becoming more likely as eigenvalues become degenerate and eigenmodes become broader in size. For  $\kappa < \kappa_c$  the correlations broaden very quickly and are lost for values smaller than about  $(\kappa_c - 0.02)$ . For  $\kappa > \kappa_c$  the correlations become sharper until  $\kappa = \kappa_{\max}$  for which the correlations are strongest. For  $\kappa > \kappa_{\max}$  the correlations broaden again.

Eigenmodes of 12-sweep cooled configurations show a different behaviour depending on whether they belong to eigenvalues on the left or right-hand side of the rhomboid-shaped eigenvalue spectrum of a cooled configuration as seen in Fig. 5. Eigenmodes belonging to the left-hand side of the eigenvalue spectrum are strongly localised and show the same behaviour as eigenmodes of hot

configurations. Eigenmodes belonging to the right-hand side of the eigenvalue spectrum are very weakly localised, but are still correlated to topology. This suggests that those eigenmodes correspond to very high eigenmodes in a hot configuration, which are lowered by cooling.

The value of  $\kappa$  where the weakly localised eigenmodes set in becomes smaller with cooling. This supports the idea of high values of  $\kappa$  corresponding to localisations on small topological objects. Small topological objects are removed first under improved cooling thus eigenmodes for high values of  $\kappa$  are the first ones to lose the strong localisation.

When an instanton model is fitted to the eigenmode density, using Eq. (4), and to the topological charge density, using Eq. (3), strongly localised eigenmodes have about the same size for  $\rho$  as the correlated topological objects. For  $\kappa_{\max}$  eigenmodes are slightly smaller than the correlated topological and for  $\kappa$  smaller than  $\kappa \approx \kappa_{\max} - 0.02$  eigenmodes are slightly larger.

On a single instanton configuration the correlation to the instanton persists strongly only for the lowest eigenmode and is then gradually lost for higher eigenmodes. On SU(3) background fields we see correlation for the 20 lowest eigenmodes. There is only little broadening which suggests that the correlation will persist for eigenmodes higher than 20.

For hot configurations these correlations allow us to “see through” the noise to underlying topological objects. This enables one to track the movement of these objects as a function of cooling.

Future work will examine the manner in which the eigenvalue spectrum is modified under improved fermion actions. In particular we plan to examine the effects of using APE-smearred fat-links in the irrelevant operators of fermion actions.

## Acknowledgements

We would like to thank the Australian National Computing Facility for Lattice Gauge Theory for time on its supercomputer Orion and Paul Coddington, Ramona Adorjan and Francis Vaughan for their technical support of this work. We would like to thank Paul Rakow and Alex Kalloniatis for useful discussions. DJK wants to thank the Baden-Württemberg-South Australia exchange program for supporting his stay in Adelaide. This research was supported by the Australian Research Council.

## References

- [1] D. Smith, H. Simma, M. Teper, *Nucl.Phys.Proc.Suppl.* **63** (1988) 558–560
- [2] H. Simma, D. Smith, *Conference Proceedings, 31st International Symposium Ahrenshoop on the Theory of Elementary Particles* (Buckow, 1997)
- [3] R.G. Edwards, U.M. Heller, R. Narayanan, *Nucl.Phys. B* **522** (1998) 285–297
- [4] R.G. Edwards, U.M. Heller, R. Narayanan, *Nucl.Phys. B* **535** (1998) 403–422
- [5] K. Jansen, C. Liu, H. Simma, D. Smith, *Nucl.Phys.Proc.Suppl.* **53** (1997) 262–265
- [6] T. DeGrand, A. Hasenfratz, hep-lat/0012021
- [7] R.G. Edwards, U.M. Heller, R. Narayanan, *Nucl.Phys.* **B540** (1999) 457–471
- [8] T. Kalkreuter, H. Simma, *Comput.Phys.Commun.* **93** (1996) 33–47
- [9] C. Gattringer, M. Göckeler, C.B. Lang, P.E.L. Rakow, A. Schäfer, hep-lat/0108001
- [10] S. Bilson-Thompson, F.D.R. Bonnet, D.B. Leinweber, A.G. Williams, hep-lat/0112034
- [11] P. de Forcrand, M.G. Perez, I.-O. Stamatescu, *Nucl.Phys.* **B499** (1997) 409; P. de Forcrand, M.G. Perez, J.E. Hetrick, I.-O. Stamatescu, hep-lat/9802017
- [12] F.D.R. Bonnet, D.B. Leinweber, A.G. Williams, J.M. Zanotti, hep-lat/0106023
- [13] <http://www.physics.adelaide.edu.au/cssm/lattice/>
- [14] H. Neuberger, *Phys.Rev.* **D61** (2000) 085015; P. Hernandez, K. Jansen, M. Luscher, *Nucl.Phys* **B552** (1999) 363–378